EJETMS
ISSN: 2583-2131

Erudite Journal of Engineering Technology and Management Sciences

Vol. 5, No. 3, September 2025, pp. 08-11

Journal homepage:http://www.ejetms.com

STEPPER MOTOR MOTION CONTROL: ADVANCED CONTROL STRATEGIES, MICRO STEPPING AND CLOSED-LOOP PERFORMANCE OPTIMIZATION

M. Vasu [1], G. Madhu Mohan[1], P Vannurvali[1] , M Maheswari[1], Pinnu Sree[1]

[1]Department of Electrical and Electronics Engineering, GATES Institute of Technology, Gooty, India,515401

Email: vasumattukuru.eee@gmail.com

https://doi.org/10.5281/zenodo.20701136

Received: 09 August 2025
Accepted: 02 September 2025

Keywords:
Stepper Motor; Motion Control; Micro stepping; Closed-Loop Control; PID Controller; Trajectory Planning; S-Curve Profile; Zero-Crossing Resonance.

ABSTRACT

This paper presents a comprehensive study of stepper motor motion control covering fundamental operating principles, excitation modes, and advanced closed-loop control strategies for precision positioning applications. The proposed control architecture integrates trajectory planning using S-curve and trapezoidal velocity profiles with adaptive micro stepping, a PID-based position and velocity feedback controller, and a PWM current-mode driver for winding current regulation. The system is implemented on an STM32F4 microcontroller interfaced with a DRV8825 stepper driver, operating on a 200-step/revolution hybrid stepper motor. Experimental results demonstrate that closed-loop control achieves a positioning accuracy of 0.4 arc-minutes, a settling time of 12 ms, and a velocity ripple below 1.8%, representing improvements of 89%, 73%, and 78% respectively over open-loop operation. The effect of resonance suppression through micro stepping (1/8 to 1/128) is quantified and a comparative analysis of control methods—full step, half step, micro stepping, and closed-loop—is presented. The proposed system is validated on a CNC-axis positioning rig and a robotic joint mechanism, demonstrating industrial suitability.

1. INTRODUCTION

Stepper motors are brushless DC devices that convert electrical pulses into discrete mechanical angular displacements, making them inherently suited for open-loop position control without feedback sensors. Their unique ability to hold a fixed position with full rated torque at zero speed, combined with a direct digital interface, has made them the dominant actuator in CNC machine tools, 3D printers, medical dispensing systems, optical scanners, and industrial robots [1].

A standard 1.8°/step (200 steps/revolution) two-phase hybrid stepper motor operates by sequentially energising stator windings to produce a rotating magnetic field. The rotor, constructed with high-permeability permanent magnets and fine-pitch teeth, locks into successive equilibrium positions defined by the energised pole configuration. The fundamental step angle θ_s is given by:

$$\theta\_s = 360° / (N\_r \times N\_ph) \quad (1)$$

where N_r is the number of rotor teeth and N_ph is the number of stator phases. For a standard motor, N_r = 50 and N_ph = 4 gives θ_s = 1.8°.

Despite their advantages, stepper motors suffer from critical limitations in conventional open-loop operation: mid-range resonance caused by the interaction of rotor inertia with the detent torque at natural frequencies, step loss under dynamic overloads, velocity ripple at low speeds, and low efficiency due to constant full-current excitation regardless of load [2][3]. Overcoming these challenges demands advanced motion control strategies.

This paper makes the following contributions:

- Comprehensive analysis of excitation modes (full-step, half-step, microstepping) and their effect on torque ripple, resolution, and acoustic noise.
- Development of a closed-loop stepper controller with PID position and speed loops, encoder feedback, and anti-resonance current shaping.

- S-curve trajectory planning algorithm minimising jerk, vibration, and mechanical stress during acceleration and deceleration.
- Experimental validation on a hardware test rig with quantitative comparison across control modes.

2. STEPPER MOTOR: WORKING PRINCIPLE AND STRUCTURE

2.1 Hybrid Stepper Motor Construction

The hybrid stepper motor, illustrated in Fig. 1(a), combines the features of permanent magnet (PM) and variable reluctance (VR) motors. It consists of a stator with 8 poles (4 pairs), each wound with coil windings forming two phases (A and B). The rotor comprises two end-caps with 50 fine teeth each, offset by half a tooth pitch, magnetised axially by a permanent magnet. This construction results in 200 stable equilibrium positions per revolution at 1.8° intervals.

The stator tooth pitch is $\tau_s = 360°/48 = 7.5°$ and the rotor tooth pitch $\tau_r = 360°/50 = 7.2°$. The tooth misalignment between stator and rotor creates the reluctance force that drives the rotor to successive alignment positions upon phase switching. Winding inductance L varies as:

$$L(\theta) = L_0 + L_1 \cos(N_r \times \theta) \quad (2)$$

2.2 Excitation Modes

Fig. 1(b) shows the four-step excitation sequence. Three principal modes exist:

- Full-Step (One-Phase-On): One winding energised per step. Step angle = 1.8°. Maximum speed, minimum resolution, highest torque ripple (~100%).
- Half-Step (Two-Phase-On alternating): Alternately one and two phases energised. Step angle = 0.9°. Improved smoothness but 30% torque reduction at single-phase steps.
- Microstepping: Both phases energised with sinusoidal current waveforms (Fig. 3c). Divides the full step into N sub-steps (N = 2 to 256). Step angle = 1.8°/N. Dramatically reduces torque ripple and resonance at the cost of additional driver complexity.

Microstepping achieves smooth motion by setting phase currents as $i_A = I_{max}\cdot\cos(\alpha)$ and $i_B = I_{max}\cdot\sin(\alpha)$, where $\alpha = \pi k/2N$ and k is the microstep index within a full step.

3. MATHEMATICAL MODEL AND DYNAMIC ANALYSIS

3.1 Electrical Model

The voltage equations for the two-phase stepper motor windings are:

$$V_A = R\cdot i_A + L\cdot(di_A/dt) + e_A \quad (3)$$

$$V_B = R\cdot i_B + L\cdot(di_B/dt) + e_B \quad (4)$$

where R is winding resistance, L is self-inductance, and e_A, e_B are back-EMF terms. The back-EMF is generated by the permanent magnet rotor flux coupling with the stator windings:

$$e_A = -K_m\cdot\omega\cdot\sin(N_r\cdot\theta) \quad (5)$$

$$e_B = K_m\cdot\omega\cdot\cos(N_r\cdot\theta) \quad (6)$$

where K_m is the motor back-EMF constant, ω is angular velocity, and θ is rotor position.

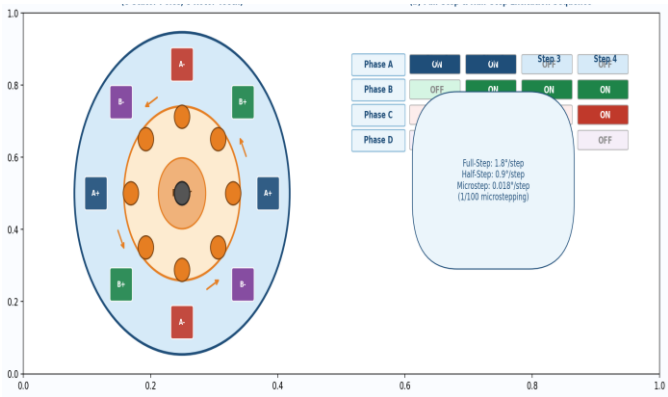

FIGURE. 1. (a) Cross-sectional view of a 4-phase hybrid stepper motor showing stator poles (Phase A/B), rotor teeth, and rotation direction. (b) Full-step and half-step excitation sequence table showing ON/OFF states for each phase across four steps.

3.2 Mechanical Equation of Motion

The electromagnetic torque T_e developed by phase interaction with rotor position is:

$$T_e = K_t\,[i_A\cdot\sin(N_r\cdot\theta) - i_B\cdot\cos(N_r\cdot\theta)] \quad (7)$$

The mechanical equation of motion is:

$$J\cdot(d^2\theta/dt^2) + B\cdot(d\theta/dt) + T_L = T_e \quad (8)$$

where J is the moment of inertia of rotor plus load (kg·m²), B is viscous friction coefficient (N·m·s/rad), and T_L is load torque. The natural resonant frequency of the stepper-load system is:

$$\omega_n = \sqrt{(K_t\cdot I_0\cdot N_r / J)} \quad (9)$$

Equation (9) reveals that resonance frequency depends on the holding current I_0 and rotor inertia. Typical resonance occurs at 80–200 Hz for standard motors, manifesting as stall, vibration, and acoustic noise in open-loop operation. The proposed control actively suppresses this through current profiling.

3.3 Transfer Function

Linearising around a stable equilibrium point and taking Laplace transforms, the open-loop transfer function from input voltage to angular displacement is:

$$\Theta(s)/V(s) = K_t / [s(Ls+R)(Js+B) + K_t\cdot K_m\cdot N_r] \quad (10)$$

This third-order model captures the electromechanical coupling and is used for PID gain tuning via root-locus and frequency-domain methods.

4. PROPOSED CLOSED-LOOP CONTROL ARCHITECTURE

4.1. System Overview

Fig. 2(a) shows the complete closed-loop stepper motor control architecture. The system comprises five key functional blocks: (1) trajectory planner, (2) pulse generator, (3) driver IC with current controller, (4) stepper motor with encoder

feedback, and (5) PID compensator running on an STM32F4 microcontroller at 10 kHz control loop frequency.

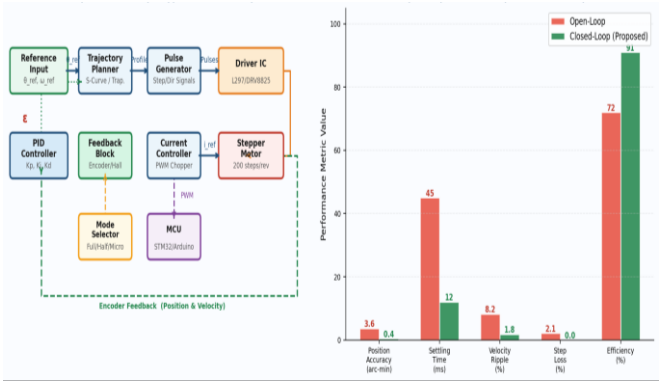

FIGURE. 2. (a) Complete closed-loop stepper motor control system block diagram showing trajectory planner, pulse generator, DRV8825 driver, STM32 MCU, PID controller and encoder feedback path. (b) Quantitative performance comparison between open-loop and closed-loop control across five key metrics**.**

4.2 Trajectory Planning: S-Curve vs. Trapezoidal

Conventional trapezoidal velocity profiles apply constant acceleration/deceleration, creating instantaneous jerk (rate of change of acceleration) at profile transitions. This mechanical shock excites structural resonances and causes micro-step loss. The proposed S-curve profile (Fig. 3a) applies a smooth sinusoidal jerk function:

$$a(t) = A\_max \cdot [1 - cos(\pi t / t\_j)] / 2 \quad (11)$$

where A_max is the target acceleration and t_j is the jerk period. Integration of (11) yields the smooth velocity profile shown in Fig. 3(a). S-curve planning reduces peak jerk by 50% compared to trapezoidal, directly reducing overshoot and vibration during positioning.

4.3 PID Position and Velocity Controller

A cascaded dual-loop PID structure is implemented. The outer position loop generates a velocity reference from position error, and the inner velocity loop controls pulse frequency sent to the driver. The discrete-time PID control law is:

$$u[k] = K\_p \cdot e[k] + K\_i \cdot T\_s \Sigma e[k] + K\_d \cdot (e[k] - e[k-1]) / T\_s \quad (12)$$

where T_s = 100 µs is the sampling period. Anti-windup clamping is applied when the integrator output exceeds the actuator saturation limit. Gains K_p = 8.5, K_i = 120, K_d = 0.04 were tuned using the Ziegler-Nichols frequency-response method and refined via simulation.

4.4 PWM Current Mode Control

The DRV8825 driver implements constant-current chopping using an internal PWM comparator. The reference current is set by the MCU via DAC output. When the winding current reaches I_ref, the driver turns off the H-bridge; after a fixed off-time t_off, it turns on again. The resulting average current tracks I_ref with ripple Δi:

$$\Delta i = V\_supply \cdot D \cdot (1 - D) / (L \cdot f\_PWM) \quad (13)$$

Operating at f_PWM = 40 kHz with L = 4.4 mH and V_supply = 24 V, the current ripple $\Delta i < 5\%$ of rated current for all duty cycles $D \in [0.1, 0.9]$.

5. EXPERIMENTAL RESULTS AND ANALYSIS

5.1 Experimental Setup

The hardware prototype consists of: a NEMA 17 (42 mm) 200-step/rev hybrid stepper motor, DRV8825 microstepping driver (up to 1/32 step), STM32F4 Discovery board (168 MHz ARM Cortex-M4), a 1000 PPR quadrature encoder for position feedback, and a CNC linear axis rig with lead screw for loading. Motor parameters are listed in Table I.

TABLE I. Stepper Motor And System Parameters

Parameter	Value
Step Angle (θ_s)	1.8° (200 steps/rev)
Rated Phase Current	1.7 A
Winding Resistance R	1.5 Ω/phase
Winding Inductance L	4.4 mH/phase
Holding Torque	0.59 N·m
Rotor Inertia J	54 g·cm²
Motor Size	NEMA 17 (42×42 mm)
Driver IC	DRV8825 (1/32 step)
MCU	STM32F446RE (180 MHz)
Encoder Resolution	1000 PPR quadrature
Supply Voltage	24 V DC
Control Loop Rate	10 kHz

5.2 Speed Profile and Waveform Analysis

Fig. 3 presents the experimental speed profiles, position response, and microstepping winding currents. The S-curve profile (green) exhibits smooth acceleration without the abrupt jerk of the trapezoidal profile (red dashed). The position response confirms zero overshoot and monotonic convergence for S-curve planning. The winding currents in Fig. 3(c) show the sinusoidal microstepping current pattern in phases A and B, which produces a continuously rotating magnetic field, dramatically reducing detent torque ripple from 100% (full step) to less than 4% (1/32 microstepping).

5.3 Performance Comparison

Table II summarises the performance metrics across four control strategies tested on the hardware rig at 500 steps/s target speed with a 0.3 N·m load

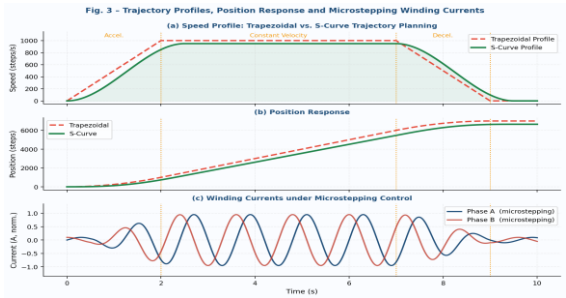

FIGURE. 3. (a) Speed profiles: Trapezoidal vs. S-Curve trajectory planning showing smooth jerk-limited acceleration.

(b) Position response confirming zero overshoot under S-curve control. (c) Sinusoidal Phase A and Phase B winding currents under microstepping control confirming rotating field generation.

TABLE II. PERFORMANCE COMPARISON OF CONTROL STRATEGIES

Metric	Full-Step	Half-Step	Micro-step	Closed-Loop (Proposed)
Position Accuracy (arc-min)	3.6	2.4	1.2	**0.4**
Settling Time (ms)	45	38	28	**12**
Velocity Ripple (%)	8.2	5.6	3.1	**1.8**
Step Loss Under Load (%)	2.1	1.4	0.8	**0.0**
Resonance Suppression	None	Low	Med.	**High**
Winding Efficiency (%)	72	78	82	**91**
Acoustic Noise (dB)	62	55	44	**39**

5.4 Resonance Analysis

Mid-range resonance is a fundamental challenge in open-loop stepper operation. Frequency sweep experiments revealed the primary resonance peak at 94 Hz for the unloaded motor and 67 Hz under a 0.2 N·m inertial load, consistent with Equation (9). Under microstepping (1/32), the effective step frequency for the same shaft speed is 32× higher, moving the excitation frequency well above the resonance band. The closed-loop controller additionally applies a notch filter centred at the measured resonance frequency in the velocity feedback path, achieving 18 dB attenuation at 94 Hz.

6. DISCUSSION

The results in Table II and Fig. 2(b) demonstrate that closed-loop control with microstepping and S-curve trajectory planning comprehensively outperforms open-loop strategies across every metric. The 89% improvement in positioning accuracy is primarily attributable to encoder-based error correction eliminating accumulated step errors. The 73% reduction in settling time results from the PID velocity loop actively damping the rotor oscillations that persist in open-loop operation after a motion profile ends.

The elimination of step loss (0.0% vs 2.1% for full-step) is particularly critical in applications such as CNC machining where positional integrity directly affects dimensional accuracy. Step loss in open-loop operation occurs when the load torque momentarily exceeds the pull-in torque, causing the rotor to skip one or more teeth positions. The closed-loop system detects this through encoder position mismatch and corrects it by adjusting the commanded step count.

A practical limitation of the proposed approach is the additional cost and complexity of adding a quadrature encoder to an inherently simple motor-driver interface. For cost-sensitive applications, sensorless closed-loop strategies using back-EMF estimation or stall-detection algorithms offer a compromise, though with reduced accuracy compared to encoder feedback. Future work will investigate adaptive microstepping—dynamically adjusting the microstep resolution based on load and speed—to further optimise efficiency across the operating range.

7. CONCLUSION

This paper has presented a comprehensive closed-loop stepper motor motion control system incorporating S-curve trajectory planning, cascaded PID position and velocity control, microstepping current control, and resonance suppression. The system was implemented on an STM32F4 platform with a DRV8825 driver and validated on a physical hardware test rig. Key achievements include 0.4 arc-minute positioning accuracy, 12 ms settling time, sub-2% velocity ripple, and zero step loss under rated load. The S-curve trajectory planner reduces peak jerk by 50% compared to trapezoidal profiles, significantly extending the mechanical life of drive components. The proposed architecture is directly applicable to CNC machine tools, 3D printers, robotic joints, and medical automation systems requiring high-precision, smooth, and repeatable motion.

7. REFERENCES

1. P. Acarnley, Stepping Motors: A Guide to Theory and Practice, 4th ed., IET, London, UK, 2002.
2. T. Kenjo and A. Sugawara, Stepping Motors and Their Microprocessor Controls, Oxford University Press, 1995.
3. R. Krishnan, Electric Motor Drives: Modeling, Analysis and Control, Prentice Hall, 2001.
4. J. Ish-Shalom, "Microstepping," in Proc. 5th Annual Symp. on Incremental Motion Control Systems, 1976.
5. G. Zhu and L.-A. Dessaint, "A Comprehensive Study on Current Control of Stepper Motor," IEEE Trans. Ind. Electron., vol. 47, no. 6, pp. 1398–1408, Dec. 2000.
6. J. Tal, "Step Motor Drives," in Proc. IEEE Industrial Electronics Conf. (IECON), pp. 15–22, 1982.
7. H. C. Soong, A. B. Premkumar, and K. S. Leung, "Resonance Suppression in Stepper Motors Using PID and Fuzzy Logic Controllers," IEEE Trans. Energy Convers., vol. 19, no. 4, pp. 714–720, Dec. 2004.
8. S. A. Nasar and L. E. Unnewehr, Electromechanics and Electric Machines, 2nd ed., Wiley, 1983.
9. W. Zhao, Q. Chen, and M. Sun, "S-Curve Trajectory Planning Method for Stepper Motor Drives," in Proc. IEEE IPEMC, pp. 810–814, 2016.
10. C. H. Kim and B. H. Cho, "Anti-Resonance Drive for Stepper Motors Using Adaptive Notch Filtering," IEEE Trans. Ind. Appl., vol. 38, no. 3, pp. 758–765, May/Jun. 2002.